Origin and significance of Si and O isotope heterogeneities in Phanerozoic, Archean, and Hadean zircon

Dustin Trail[1,2,*], Patrick Boehnke[3,4], Paul S. Savage[5],

Ming-Chang Liu[2], Martha L. Miller[1], Ilya Bindeman[6]

[1]Department of Earth & Environmental Sciences
University of Rochester, Rochester, NY 14627, USA

[2]Department of Earth, Planetary and Space Sciences,
University of California, Los Angeles, CA, USA

[3]Department of the Geophysical Sciences,
The University of Chicago, Chicago, IL 60637

[4]Chicago Center for Cosmochemistry, Chicago, IL

[5]School of Earth and Environmental Sciences,
University of St Andrews, UK

[6]Department of Earth Sciences,
University of Oregon, Eugene, OR, 97403, USA

* dtrail@ur.rochester.edu; ph 585 276 7182

Classification PHYSICAL SCIENCES: Earth

Abstract Hydrosphere interactions and alteration of the terrestrial crust likely played a critical role in shaping Earth's surface, and in promoting prebiotic reactions leading to life, before 4.03 Ga (the Hadean Eon). The identity of aqueously-altered material strongly depends on lithospheric cycling of abundant and water-soluble elements such as Si and O. However, direct constraints that define the character of Hadean sedimentary material are absent because samples from this earliest eon are limited to detrital zircons ($ZrSiO_4$). Here we show that concurrent measurements of Si and O isotope ratios in Phanerozoic and detrital pre-3.0 Ga zircon constrain the composition of aqueously-altered precursors incorporated into their source melts. Phanerozoic zircon from (S)edimentary-type rocks contain heterogenous $\delta^{18}O$ and $\delta^{30}Si$ values consistent with assimilation of metapelitic material, distinct from the isotopic character of zircon from (I)gneous- and (A)norogenic-type rocks. The $\delta^{18}O$ values of detrital Archean zircons are heterogenous, though yield Si isotope compositions like mantle-derived zircon. Hadean crystals yield elevated $\delta^{18}O$ values (vs. mantle zircon) and $\delta^{30}Si$ values span almost the entire range observed for Phanerozoic samples. Coupled Si and O isotope data represent a new constraint on Hadean weathering and sedimentary input into felsic melts including re-melting of amphibolites possibly of basaltic origin, and fractional addition of chemical sediments, such as cherts and/or Banded Iron Formations (BIFs) into source melts. That such sedimentary deposits were extensive enough to change the chemical signature of intracrustal melts suggests they may have been a suitable niche for (pre)biotic chemistry as early as 4.1 Ga. **(248 words)**

Key words; Hadean; zircon; weathering; Silica cycle; origin of life; Lachlan Fold Belt

Significance

The crust or its chemically weathered derivatives likely served as a substrate for the origin of life, which could have occurred by 4.1 Ga. Yet no known *bona fide* terrestrial rocks from this time remain. Studies have thus turned to geochemical signatures within detrital zircons from this time. While zircons do not directly record low-temperature weathering processes, they inherit isotopic information upon recycling and re-melting of sediment. We developed a method to fingerprint the identity of material involved in water-rock interactions >4 Ga, bolstered by a large Si and O isotopic dataset of more modern zircon samples. The data presented here provide evidence for chemical sediments, such as cherts and Banded Iron Formations on Earth >4 Ga. **(117 words)**

\body

Introduction

In the apparent absence of a pre-4.0 Ga terrestrial rock record, early speculations about the Hadean Earth (~4.5-4.0 Ga) were drawn from meteorites and backward extrapolation of preserved Archean rocks. Insights into the nature of the Hadean surface environment relied on broad estimates of mantle heat production and its transport to the surface, and scaling of the lunar impact record to the early Earth (1). Laboratory simulations predicted intense meteorite bombardment and a thick steam-rich atmosphere (2), suggesting that Earth may not have been continuously habitable in the first 500 Myr (3).

The first direct constraints on the geology of the young Earth came from the discovery of Hadean detrital zircons (4). Subsequent *in situ* oxygen isotope measurements of some Hadean

zircon yielded isotopically heavy compositions, relative to the canonical mantle value (5,6). Such isotopic shifts provide evidence for water-rock interactions at low temperatures (sensu lato), followed by re-melting and incorporation of these signatures into Hadean zircon parent melts by 4.2 to 4.3 Ga (5-8). More recent numerical calculations that evaluate early Earth heat transfer and plausible chemical reactions (9), the thermal effects of terrestrial impact metamorphism (10), and a re-evaluation of lunar impact chronology (11) continue to strengthen the case a continuously habitable planet shortly after accretion.

Such discoveries are important, although many uncertainties remain regarding Earth's earliest development. This highlights the need to find new ways to better constrain Earth's primordial geology. For instance, only limited information about the identity of weathered material involved in the zircon source melt is provided by mildly elevated Hadean $\delta^{18}O$ values, which are up to ~2 ‰ above present-day mantle zircon. This is because almost all surficial/low-temperature water-rock interactions result in an isotopically heavy O composition being imparted on the rock. Constraining the identity of weathered Hadean material is timely due to the suggestion that an isotopically light carbon inclusion in a ~4.1 Ga zircon may indicate the presence of a biosphere (12), implying the need for a suitable substrate for life by this time.

Silicon isotopes, like O isotopes, are also strongly fractionated during chemical weathering of silicate material or low temperature water-rock interactions (SI Appendix, Fig. S1). Given the dominance of O and Si in the lithosphere, the composition of altered or weathered products strongly depends on reactions that involve both elements. First, consider that neoformation of clay minerals prefers the lighter Si isotopes, and the degree of fractionation is magnified with the extent of weathering degree/amount of desilicification to more negative $\delta^{30}Si$ values (i.e. 1:1 clays such as kaolinite are much lighter than 2:1 clay minerals, 13-15). This

gives Si isotopes the added advantage over O isotopes alone as they have the potential to be a definitive proxy for identifying the presence of pelitic sediment in a melt source (Fig. 1, path 1). Second, unlike O isotopes, Si isotopes are unaffected during hydration of primary silicates (i.e. serpentinization) and at low weathering degrees, where igneous minerals still dominate the Si isotope signature (16; Fig. 1, path 2). Third, precipitation and diagenesis of authigenic silica and hydrothermal silicification can lead to large variations in δ^{30}Si (17-19). Under non-equilibrium conditions, this can generate negative shifts in δ^{30}Si, but unlike desilicification, often there may be no correlation between Si and O variations in the silica, due to the different behavior of these elements under different rock/water ratios and temperatures (18). Finally, Si isotopes have another advantage over O isotopes alone because seawater-derived authigenic silica (i.e., chert) reveals uniquely heavy Si isotope compositions (e.g. 20; Fig. 1, path 3). These Si-O isotope fractionation pathways – shown schematically in Figure 1 – demonstrate the critical advantage of coupled Si-O isotope analysis.

Melt assimilation of the weathered products described above may be used to explore past environments only if the isotopic composition of the whole rock (WR) and minerals – including zircon – partially, at least, reflect these original altered products. Such variations in WR Si isotope compositions, linked unequivocally to source variation, have been measured in several localities, including the Lachlan Fold Belt (21,22). Moreover, there is limited Si isotope fractionation caused by partial melting and igneous fractional crystallization; mantle rocks and mantle-derived melts yield identical δ^{30}Si values (Bulk Silicate Earth δ^{30}Si = -0.29 ± 0.07‰ relative to NBS28; 15). Felsic rocks, absent of any non-igneous assimilant, tend to be only 0.10 to 0.20 ‰ heavier than BSE, demonstrating there is a small and crucially predictable enrichment of heavier Si isotopes due to magmatic differentiation (23). A source rock signature will be

recorded in zircons, provided that the difference between $\delta^{30}Si$(WR) and $\delta^{30}Si$(zircon) – i.e., $\Delta^{30}Si$(WR-zircon) – is constrained.

To extend the terrestrial Si isotope record back to the Hadean, we take the approach that $\delta^{30}Si$ values should be considered with $\delta^{18}O$, because such coupled isotopic analyses are potentially powerful in identifying the lithologies assimilated in Hadean melt sources (Fig. 1). In this contribution, we report solution-based multi-collector inductively coupled plasma mass spectrometry (MC-ICP-MS) measurements of mantle-derived zircon and separate felsic whole rock fractions from the crust to define: (i) the Si isotopic composition of zircon that crystallized in the absence of sediment inputs; and (ii) $\Delta^{30}Si$(WR-zircon), which constrains high temperature Si isotope fractionations. To analyze single zircons at ~20 μm spatial resolution, we developed an ion microprobe analytical protocol for simultaneous *in situ* measurements of both isotope systems. First, this method was used to investigate coupled Si and O isotope compositions of *in-context* igneous zircons from 10 different Australian Lachlan Fold Belt (LFB) Phanerozoic granitoids classified as (S)edimentary, (I)gneous, and (A)norogenic (SI Appendix, Fig. S2). These data, together with the Si and O isotope record of Eoarchean sediments (17,20), form the basis for our interpretation of ion microprobe data for Hadean and Archean zircon. An overview of measured samples is presented in SI Appendix, Table S1.

Results

Mantle-derived Mud Tank carbonatite (Australia), Kimberley pool (South Africa), and Orapa Kimberlite (Botswana) zircons yield $\delta^{30}Si_{NBS28}$ values that range from -0.34 to -0.41 ‰ (SI Appendix, Table S2). The average $\delta^{30}Si$ value of -0.38±0.02 ‰ (1 s.d.), determined by MC-ICP-MS, is used to define $\delta^{30}Si$ of mantle-derived zircon. The LFB Jindabyne tonalite fractions

yield respective δ^{30}Si values for zircon, WR, and quartz of -0.57±0.02, -0.20±0.03, and -0.11±0.02 ‰. This defines Δ^{30}Si(WR-zircon) = 0.37 ‰ for this sample (Fig. 2), in good agreement with *ab initio* Si isotope fractionation calculations (24).

Ion microprobe zircon Si isotope data reveal differences, albeit with overlap, between our Australian LFB granitoid types (Fig. 3; SI Appendix, Table S3). Typically, S-type samples contain δ^{30}Si values that extend to more negative values than I- or A-type granitoids. In the most extreme cases, zircon δ^{30}Si extends down to about -1.5 ‰, as observed for the Cootralantra samples. Zircons analyzed from the Bullenbalong S-type granitoid are not characterized by δ^{30}Si values lighter than -1.0 ‰, and in fact the overall distribution of δ^{30}Si makes it broadly comparable to the δ^{30}Si range of other I-type zircons. The Cowra Granodiorite contains zircon δ^{30}Si that would be most consistent with results obtained from I-type samples, except that a larger fraction of the analyses is shifted toward more negative values than other I-types examined thus far. I-type granitoids have a similar dispersion in δ^{30}Si as S-types, though zircon δ^{30}Si distributions are shifted towards heavier values, and several data are within error of 0 ‰. Except for Cowra zircons, no S-type analyses are within error of 0 ‰. The A-type sample (Watergums) and Duluth Gabbro yield tighter δ^{30}Si distributions when compared to I- and S-type ranges for a similar number of data points. S- and I-type O isotope data, collected 'simultaneously' with Si isotopes, also show distinct differences (Fig. 4; SI Appendix, Fig. S4). S-type zircons typically yield $\delta^{18}O_{VSMOW}$ values from +8 to 10.5 ‰, whereas I- and A-types are typically confined to δ^{18}O values of +6 to 8.5 ‰.

Individual ion microprobe spot data (n = 79) for Jack Hills zircons consist of 14 zircons ≥4.0 Ga, and 21 Archean grains (SI Appendix, Table S4), and reveal subtle isotopic differences among the two age groups (Fig. 5; SI Appendix, Fig. S4). Specifically, the Archean zircon δ^{18}O

values are between +5.2 to +6.8‰, comparable to previous Jack Hills zircon studies (25). The δ^{30}Si values of Archean zircon are broadly confined to those like mantle-derived zircon. Most Hadean samples yield δ^{18}O values that range from +6 to 7 ‰ and same grains exhibit both enrichments and depletions in ^{30}Si relative to mantle zircon and show a broadly similar range as Phanerozoic zircon.

Discussion

Phanerozoic 'in-context' zircons

The well-studied Lachlan Fold Belt represents an ideal test target to demonstrate *in situ* zircon-scale investigations. Coupled Si and O isotope studies of zircon have not been conducted previously, so an obvious question is whether these zircon data lead to broadly similar interpretations when compared to WR geochemical studies. The WR Si isotope data show that S-type granitoids are, on average, isotopically lighter than I- and A-type samples, although the range of Si isotopes in S-type granitoid WR extends to lower and slightly higher δ^{30}Si values than the other two granitoid types (21; SI Appendix, Fig. S1).

Using felsic rock isotope fractionation relationships of Δ^{18}O(WR-zircon) ≈ 2 ‰ (27), and Δ^{30}Si(WR-zircon) ≈ 0.37‰ (see Fig. 2) we find that S-type zircon, on average, predicts the most negative WR δ^{30}Si and most elevated δ^{18}O WR values. This result is consistent with assimilation of pelitic material (e.g., Fig. 1, path 1), and WR data for the region (20). For example, averaging the results from S-type Shannons Flat zircons (Fig. 3; SI Appendix, Fig. S3) predicts respective WR δ^{30}Si and δ^{18}O values of -0.45 ‰ and +10.4 ‰. A δ^{30}Si value of -0.45 ‰ is the lowest estimated WR value of the 10 granitoids explored here, and is in broad agreement with the lowest WR δ^{30}Si values so far reported in the LFB (SI Appendix, Fig. S1). Moreover, predicted

196 WR values from S-type zircons imply another sedimentary source besides Ordovician sediments
197 in close association with the LFB granitoids, also consistent with conclusions reached using WR
198 data only (21). Similar agreement is found for oxygen isotopes (28); other WR isotope
199 calculations for the different granitoids are reported in SI Appendix, Table S3. What is also
200 evident, especially for the I-type zircons, is the presence of an isotopically heavy Si source in
201 some regions of the Lachlan Fold Belt (e.g., Fig. 3; Glenbog). We speculate that this is due to
202 fractional crystallization and seawater-derived authigenic silica (Fig. 1; path 3). In the latter case,
203 silica assimilation will not drive any resulting melt into the peraluminous field nor would it be
204 likely to affect Sr and Nd isotope compositions, hence the rock will still resemble an I-type, even
205 with the anatexis of 'non-igneous' material.

206 If individual data points are considered in lieu of averages, I- and S-type zircon Si- and
207 O- isotopes imply heterogenous isotopic values for the source rocks (Fig. 4). This is particularly
208 marked when compared to histogram ranges defined by Duluth Gabbro and A-type Watergums
209 zircon Si and O isotope data (Fig. 3; SI Appendix, Fig. S3). The petrogenesis of zircon in
210 gabbros and A-type melts is typically linked to a single (generally primitive) melt composition
211 which evolved via fractional crystallization. This homogeneous, 'primitive' melt composition is
212 well reflected in both suites by their mantle-like Si isotope compositions ($\delta^{30}Si \approx -0.35‰$) and
213 normal distribution (Fig. 3). In contrast, the S- and I-type LFB zircons both define wider, often
214 non-normal, data distributions. Although the lower analytical precision of *in situ* measurements
215 contributes to the apparent range, if all zircons from each I- and S-type melt had an identical Si
216 isotope composition (with perhaps minor variations due to fractional crystallization), data
217 distributions similar to that of the A-type or gabbroic zircons are expected. Hence, the wider I-
218 and S-type zircon Si and O isotope range likely reflects heterogeneities in the source, or possibly

multiple melt sources. This incomplete homogenization of multiple source materials in the Lachlan samples is also observed in Nd, Sr, and O-isotope WR and mineral studies, which underscores the hybrid nature of felsic natural systems (28,29).

Hadean and Archean (detrital) zircons

Several zircons yield δ^{30}Si values indistinguishable from mantle-derived zircon, but with heavier δ^{18}O than the mantle (Fig. 5). These zircons may have crystallized from melts that included assimilation of hydrated/serpentinized basalt, whereby the original 'igneous' Si isotope composition of the host rocks remained unaltered, (e.g., Fig. 1, path 2). Alternatively, it was suggested that low fluid/rock ratios could generate positive O isotope excursions without accompanying Si isotope variation (19). Both scenarios are consistent with Hadean melts (partially) influenced by source material altered by considerable hydrothermal activity.

Perhaps the most intriguing Hadean zircon yields a mantle-like δ^{18}O value of +5.49 ‰, but records a δ^{30}Si value of -1.13 ‰ (grain 1-10). This grain represents our strongest evidence for a Hadean Si reservoir out of equilibrium with the mantle. Evaluation of the δ^{18}O value only would lead to the conclusion that this grain shows no evidence for interaction with an aqueous reservoir, whereas δ^{30}Si suggests otherwise. We rule out fractional crystallization, as Δ^{30}Si(WR-zircon) is ~0.35 ‰ for felsic systems; this relationship implies a WR value of ~-0.75 ‰. To explain this result, we turn to the Archean Si isotope sedimentary record.

Archean cherts, which formed by chemical precipitation (and re-precipitation), have Si isotope values as low as ~-3 ‰, which also applies to Archean BIFs (17, 30-32). These sediments are typically assumed to result in ^{18}O-enriched material compared to the mantle (20), meaning that an ^{18}O-depleted reservoir is also required to balance the mantle-like zircon value of

+5.49 ‰. The Fe-oxide phases in BIFs are one possibility; these may be ^{18}O-depleted (33), which is also supported by low temperature Fe-oxide-H_2O oxygen isotope equilibrium fractionations (34). Also, alteration of mafic rocks by seawater can either enrich or deplete the resulting product in ^{18}O; higher temperature (post-solidus) exchange with seawater decreases the $\delta^{18}O$ value of the altered rock (35,36). This reasoning assumes that seawater $\delta^{18}O$ was ~0‰, similar to modern (36), which is based on an assumed balance of hydrothermal and weathering fluxes (37). Alternatively, at far-from-equilibrium conditions (e.g., dashed arrows in Figure 1), light Si isotope compositions have been recorded in chemical precipitates where no large variations in O have been recorded (38). We propose that burial and anatexis of a succession of oceanic lithologies (cherts, BIFs and/or altered mafic rocks) as a possible explanation for the chemistry of this 4.05 Ga zircon. A simple end-member Si isotope mixing model with basalt and chemical sediment (e.g., chert) requires less than 20% of the latter to explain the range of $\delta^{30}Si$ values observed in detrital zircons (SI Appendix, Fig. S5). ±

Zircon samples in which both $\delta^{30}Si$ and $\delta^{18}O$ outside the 'mantle' zircon field are rare. The most ^{30}Si enriched detrital zircon is from a 4.05 Ga grain, which is also mildly enriched in ^{18}O relative to the mantle (grain ID = 1-9, $\delta^{30}Si$ = +0.14‰; $\delta^{18}O$ = 6.26‰). As with the positive Si isotope zircons from the LFB granites, this datum implies seawater as the dominant source of $\delta^{30}Si$ (Fig. 1, path 3); note that silicification of volcanogenic sediments from Archean samples display more positive $\delta^{30}Si$ values that range from +0.1 to 1.1 ‰, which was also linked to seawater-derived silica (20). The same study showed that Archean felsic schists are fractionated to positive $\delta^{30}Si$ values, which is also qualitatively consistent with the Si- and O- isotope data for this zircon.

Conclusions

In many cases, the Si isotopic measurements of crustal zircons with clear input of weathered material into the source magmas, as judged by ^{18}O enrichments, exhibit $\delta^{30}Si$ values indistinguishable from mantle-derived zircon. Thus, correlative analysis of Si- and O- isotopes provides a more robust interpretation than either isotopic system alone; in the case of the detrital grains, 'path 2' was the most common weathering trajectory. That said, a fraction of the Si measured in Phanerozoic, Archean, and Hadean zircon requires assimilation of silica that interacted with aqueous solutions into the melt protolith(s), ruling out Si derivation exclusively from mantle sources. The range of Si and O isotope compositions recorded in the Hadean zircons is consistent with melt generation from isotopically heterogeneous sources, similar to the migmatite-related formation of Phanerozoic 'crustal'-derived I- and S-type granites. This is also contrary to a model in which all Hadean zircon source melts were derived from isotopically homogeneous mafic rocks (39).

The combined $\delta^{18}O$ and $\delta^{30}Si$ measurements restrict the characteristics of Hadean material altered in low temperature environments. Our preferred model is that some of these involved the anatexis of chemical sediments, possibly felsic schists, and (potentially silicified) metabasalts. This is especially important because the early chemistry of the crust and aqueous solutions are important variables that almost certainly affected early prebiotic or inorganic chemical reactions (40). Archean cherts and highly metamorphosed quartz-pyroxene sediments host some of the earliest proposed evidence for life associated with rocks (41,42), and an isotopically light carbon inclusion within a Hadean zircon pushes record of a potential biosphere back to 4.1 Ga (12). Our new evidence bolsters the case for the existence of a previously

287 undocumented suite of diverse environments – including siliceous sediments – for (pre)biotic
288 chemistry to take hold in the late Hadean.

289 ## Materials and Methods

290

291 **Zircon samples**

292 'Mantle' zircons include samples from Orapa (Botswana), and Kimberley Pool, South
293 Africa (43), a megacryst from the Mud Tank carbonatite, and AS-3 zircons (45). 'Crustal'
294 zircons were extracted from 5 S-type, 4 I-type, and 1 A-type LFB hand samples with ages from
295 395 to 436 Ma (44-48). Detailed information about sample collection location and zircon
296 geochemistry – including crystallization temperatures – is presented in the SI and elsewhere
297 (50,51). Jack Hills hand samples were collected from the classic locality (5); previously
298 published U-Pb zircon ages are presented elsewhere (51). Fragments from a large crystal from
299 Kuehl Lake (KL) were also analyzed, likely from the same locality as 91500 (52).

300 **MC-ICP-MS solution-based measurements**

301 The bulk Si isotope composition was measured using solution MC-ICP-MS techniques,
302 following previously developed methods (54,55). Sample dissolution was performed using an
303 alkali fusion method. Briefly, between 2 and 10 mg of sample powder was weighed into a silver
304 crucible (99.99% purity), accompanied by ~200 mg of semiconductor grade NaOH. The crucible
305 was placed into a muffle furnace and heated for 15 minutes at 720°C. The resultant fusion cake
306 (inside the crucible) was subsequently immersed in MQ-e water (18.2 MΩ.cm), left to
307 equilibrate overnight, then transferred into pre-cleaned polypropylene bottles. The solution was
308 diluted further in MQ-e water and acidified to 1% HNO_3 v/v.

Silicon was purified for isotope analysis using a single-stage cation exchange resin ion chromatography procedure. Sample solutions were loaded on to BioRad Poly-Prep columns containing 1.8ml of pre-cleaned BioRad AG 50W-X12 cation exchange resin (200-400 mesh). As long as the sample pH is between 2-8, silicon will be in solution as a neutral or anionic species and will pass straight through the resin, eluted using MQ-e water – all other major element species will be in cationic form and are quantitatively retained by the resin.

Silicon isotopes were analyzed using a Neptune Plus (Thermo Fisher Scientific) MC-ICP-MS at both the Institute de Physique du Globe de Paris (IPGP) and at the St Andrews Isotope Geochemistry Laboratories (STAiG), University of St Andrews. The instruments were operated in medium resolution mode (to resolve and avoid polyatomic interferences), and samples were introduced into the instruments using an ESI 75µl.min^{-1} PFA microflow nebulizer and an SIS spray chamber. A sample concentration of 2 ppm typically resulted in a signal of between ~14 and 24V on the ^{28}Si beam (using 10^{11} Ω resistors), depending on the instrument. Procedural blanks ranged from between 13 and 70 mV on the ^{28}Si beam, which is negligible (<10 ppb Si) relative to the sample. Isotope ratios were measured in static mode, with each measurement consisting of 25 cycles of ~3 second integrations, with a 3 second idle time. Isotope measurements were calculated using the standard-sample bracketing method, with NBS28 (NIST RM 8546) as the bracketing standard, in permil (‰) as follows: $\delta^{x}Si = [(^{x}Si/^{28}Si_{sample} / {}^{x}Si/^{28}Si_{NBS28}) - 1] \times 1000$; where x = 30 or 29, depending on the ratio.

Solution Si isotope data are presented in SI Appendix, Table S2. Each datum is calculated as a mean of 3-5 separate measurements, and the uncertainty is calculated as the standard deviation. All paired ^{30}Si and ^{29}Si data plot on a predicted mass-dependent fractionation line (56), indicating that significant interferences on the isotope beams were resolved. Aliquots of

the standards BHVO-2 and Diatomite were consistently purified through chemistry and analyzed alongside the sample unknowns. These are also given in SI Appendix, Table S2, and are identical to their accepted values (15).

Laser fluorination O isotope measurements

Laser fluorination oxygen isotope analyses were performed at the University of Oregon using a 35W CO_2-laser in a single analytical session (Oct. 2017). Zircon fragments with weights of ~1.5 mg were reacted with purified BrF_5 reagent to liberate oxygen. The gases generated in the laser chamber were purified through a series of cryogenic traps held at liquid nitrogen temperature and a Hg diffusion pump to remove traces of fluorine gas. Oxygen was converted to CO_2 gas using a small platinum-graphite converter, and then the CO_2 gas was analyzed on a MAT 253 mass spectrometer. Four to seven aliquots of standards were analyzed together with the unknown samples during each analytical session (for detailed analytical methods, see (57)). Three UOG ($\delta^{18}O$ = +6.62 ‰) and two Gore Mt Garnet, UWG2, ($\delta^{18}O$ = +5.80 ‰) were used in the standard set (58) and varied ±0.07‰.

Ion microprobe Si and O isotope measurements

Zircons were cast in epoxy along with zircon megacryst chips and AS-3. The South African kimberlite (KIM) reproduced with the lowest standard deviation for Si isotopes by MC-ICP-MS and was thus used as our primary matrix-matched standard for ion microprobe work. Samples were gently polished by hand using disposable 1 μm Al_2O_3 polishing paper, cleaned in successive ultrasonic baths of soapy water and distilled water, dried in a vacuum oven, and then Au coated. A separate mount containing Jack Hills zircons was also prepared. Select crystals were plucked from a pre-existing mount (51), re-cast in epoxy with standards, and polished. All

354 crystals were imaged by cathodoluminescence to help guide ion microprobe spot locations (SI
355 Appendix, Fig. S4).

356 The O and Si isotopic analyses of zircons were conducted on the UCLA CAMECA
357 *ims*1290 ion microprobe. A 3 nA Cs^+ primary beam, rastering over 10×10 μm on the samples,
358 yielded sufficient secondary ion signals ($^{18}O^-$ and $^{30}Si^- \geqq 6\times10^6$ and 3×10^6 counts per second,
359 respectively) to be collected with Faraday cups (FCs) in dynamic multicollection mode. This
360 configuration allows for simultaneous measurement of $^{16}O^-$ and $^{18}O^-$ on the L'2 and H'2 FCs,
361 respectively, followed by that of $^{28}Si^-$ and $^{30}Si^-$ on C and H1 (all FCs) after one mass jump. The
362 mass resolution (M/ΔM) was set at 2,400 (exit slit #1 on the multicollection trolley) to separate
363 molecular interferences from peaks of interest. One spot analysis is composed of 20 cycles, each
364 of which includes a counting time of 4 seconds for oxygen isotopes, and of 10 seconds for Si
365 isotopes. The backgrounds of FCs were determined during the 30 second presputtering prior to
366 each analysis, and then were corrected for in the data reduction. Secondary electron images were
367 collected after analysis (SI Appendix, Fig. S7) to verify analytical spot locations were free of
368 visible inclusions and cracks. External reproducibilities obtained on the standard KIM zircons
369 were 0.11‰ for $^{18}O/^{16}O$ and 0.23‰ for $^{30}Si/^{28}Si$ (1 s.d.), which are commensurate with the
370 internal measurement errors, and better than reconnaissance O-isotope results obtained for the
371 Hyperion-II oxygen plasma source (59; SI Appendix, Fig. S7).

372

373 **Acknowledgements:**

374 This work was supported by NSF grants EAR-1447404 and EAR-1650033**.** The ion
375 microprobe facility at UCLA is partially supported by the Instrumentation and Facilities
376 Program, Division of Earth Sciences, NSF (EAR-1339051 and EAR-1734856). The LA-ICP-

MS instrument at the University of Rochester is partially supported by EAR-1545637. PB is supported by the University of Chicago Chamberlin Postdoctoral Fellowship. We thank Jacob Buettner for assistance and George Morgan for CL imaging. We thank Stephen Mojzsis and two anonymous reviewers for careful and thoughtful comments and suggestions that improved the clarity and content of the manuscript.

References:

1. Smith, JV (1981) The First 800 Million Years of Earth's History. *Phil. Trans. R. Soc. Lond. A*, 301: 401-422.
2. Sleep NH, Zahnle KJ, Kasting JF, Morowitz HJ (1989) Annihilation of ecosystems by large asteroid impacts on the early Earth. *Nature*, 342(6246): 139-142.
3. Maher KA, Stevenson DJ (1986) Impact frustration of the origin of life. *Nature*, 331: 612-614.
4. Froude DO, Ireland TR, Kinny PD, Williams IS, Compston W, Myers JS (1983) Ion microprobe identification of 4,100-4,200 Myr-old terrestrial zircons. *Nature* 304: 616-618.
5. Mojzsis SJ, Harrison TM, Pidgeon RT (2001) Oxygen-isotope evidence from ancient zircons for liquid water at the Earth's surface 4,300 Myr ago. *Nature*, 409: 178-181.
6. Valley JW, Peck WH, King EM, Wilde SA (2002) A cool early Earth. *Geology*, 30: 351-354.
7. Harrison TM (2009). The Hadean Crust: Evidence from >4 Ga Zircons. *Annual Review of Earth and Planetary Sciences*, 37: 479-505.
8. Cavosie AJ, Valley JW, Wilde SA (2005) Magmatic $\delta^{18}O$ in 4400–3900 Ma detrital zircons: a record of the alteration and recycling of crust in the Early Archean. *Earth Planet Sci Lett*, 235: 663-681.
9. Sleep, N.H., Zahnle, K., Neuhoff, P.S., (2001) Initiation of clement surface conditions on the earliest Earth. *Proc Natl Acad Sci*, 98: 3666-72.
10. Abramov O, Mojzsis SJ (2009) Microbial habitability of the Hadean Earth during the late heavy bombardment. *Nature* 459: 419-422.
11. Boehnke P, Harrison TM (2016) Illusory Late Heavy Bombardments. *Proc Natl Acad Sci* 113:10802–10806.
12. Bell, EA, Boehnke, P, Harrison, TM (2015) Potentially biogenic carbon preserved in a 4.1 billion-year-old zircon. *Proc Natl Acad Sci*, 112: 14518–14521.
13. Opfergelt S, Delmelle P (2012) Silicon isotopes and continental weathering processes: Assessing controls on Si transfer to the ocean. *Comptes Rendus Geoscience*, 344: 723-738.
14. Opfergelt, S. et al. (2012) Silicon isotopes and the tracing of desilication in volcanic soil weathering sequences, Guadeloupe. *Chemical Geology*, 326: 113-122.
15. Savage, PS, Armytage RMG, Georg RB, Halliday AN (2014) High temperature silicon isotope geochemistry. *Lithos*, 190-191: 500-519.

16. Savage PS, Georg RB, Williams HM, Halliday AN (2013) The silicon isotope composition of the upper continental crust. *Geochimica et Cosmochimica Acta* 109:384-399.
17. Marin-Carbonne J, Robert F, Chaussidon M (2014) The silicon and oxygen isotope compositions of Precambrian cherts: A record of oceanic paleo-temperatures? *Precambrian Research* 247:223-234
18. Pollington AD, *et al.* (2016) Experimental calibration of silicon and oxygen isotope fractionations between quartz and water at 250°C by in situ microanalysis of experimental products and application to zoned low δ^{30}Si quartz overgrowths. *Chemical Geology* 421:127-142.
19. Kleine BI, Stefánsson A, Halldórsson SA, Whitehouse MJ, & Jónasson K (2018) Silicon and oxygen isotopes unravel quartz formation processes in the Icelandic crust. *Geochemical Perspectives Letters*:5-11.
20. Abraham K, Hoffman A, Foley SF, Cardinal D, Harris C, Barth MG, André L (2011) Coupled silicon–oxygen isotope fractionation traces Archaean silicification. *Earth and Planet. Sci. Lett.*, 301(1-2): 222-230.
21. Savage PS et al. (2012) The silicon isotope composition of granites. *Geochimica et Cosmochimica Acta*, 92: 184-202.
22. Poitrasson F, Zambardi T (2015) An Earth–Moon silicon isotope model to track silicic magma origins. *Geochimica et Cosmochimica Acta* 167:301-312.
23. Savage PS, Georg RB, Williams, HM, Burton KW, Halliday AN (2011) Silicon isotope fractionation during magmatic differentiation. *Geochimica et Cosmochimica Acta*, 75: 6124-6139.
24. Qin T, Wu F, Wu Z, Huang F (2016) First-principles calculations of equilibrium fractionation of O and Si isotopes in quartz, albite, anorthite, and zircon. *Contributions to Mineralogy and Petrology* 171(11) 10.1007/s00410-016-1303-3.
25. Bell EA, Harrison TM, McCulloch MT, Young ED (2011) Early Archean crustal evolution of the Jack Hills Zircon source terrane inferred from Lu–Hf, 207Pb/206Pb, and δ18O systematics of Jack Hills zircons. *Geochimica et Cosmochimica Acta*, 75: 4816-4829.
26. Valley JW, Kinny PD, Schulze DJ, Spicuzza MJ (1998) Zircon megacrysts from kimberlite: oxygen isotope variability among mantle melts. *Contrib Mineral Petrol* 133:1-11.
27. Trail D, Bindeman IN, Watson EB, Schmitt AK (2009) Experimental calibration of oxygen isotope fractionation between quartz and zircon. *Geochimica et Cosmochimica Acta*, 73: 7110-7126.
28. O'Neil JR, Chappell BW (1977) Oxygen and hydrogen isotope relations in the Berridale batholith. *J. geol. Soc. Lond.*, 33: 559-57
29. Chappell BW, White AJR (1992) I- and S-type granites in the Lachlan Fold Belt. *Transactions of the Royal Society of Edinburgh: Earth Science*s 83: 1-26.
30. André L, Cardinal, D, Alleman L, Moorbath S. (2006) Silicon isotopes in ~3.8 Ga West Greenland rocks as clues to the Eoarchaean supracrustal Si cycle. *Earth and Planetary Science Letters*, 245: 162-173.
31. Robert F, Chaussidon M. (2006) A palaeotemperature curve for the Precambrian oceans based on silicon isotopes in cherts. *Nature*, 443: 969-72.

32. Steinhoefel G, Horn I, von Blanckenburg F (2009) Micro-scale tracing of Fe and Si isotope signatures in banded iron formation using femtosecond laser ablation. *Geochimica et Cosmochimica Acta*, 73: 5343-5360.
33. Khan RMK, Sharma SD, Patil DJ, Naqvi S.M. (1996) Trace, rare-earth element, and oxygen isotopic systematics for the genesis of banded iron-formations: Evidence from Kushtagi schist belt, Archaean Dharwar Craton, India. *Geochimica et Cosmochimica Acta*, 60: 3285-3294.
34. Zheng, YF (1991) Calculation of oxygen isotope fractionation in metal oxides. *Geochim. Cosmochim. Acta*, 55: 2299-2307.
35. Wenner DB, Taylor Jr, HP (1973) Oxygen and hydrogen isotope studies of the serpentinization of ultramafic rocks in oceanic environments and continental ophiolite complexes. *American Journal of Science*, 273: 207-239.
36. Muehlenbachs K, Clayton, RN (1976) Oxygen Isotope composition of the oceanic crust and its bearing on seawater. *J. of Geophys. Res.* 81, 4365-4369.
37. Holland, HD (1984) The Chemical Evolution of Atmospheres and Oceans. *Princeton Univ. Press*, pp. 587.
38. Brengman LA (2015) Distinguishing primary versus secondary geochemical and silicon isotope characteristics of Precambrian chert and iron formation. *Univ. Tennessee PhD thesis 238 pp*.
39. Kemp AIS, et al. (2010) Hadean crustal evolution revisited: New constraints from Pb–Hf isotope systematics of the Jack Hills zircons. *Earth and Planetary Science Letters* 296:45-56.
40. Benner SA, Kim H-J, Carrigan MA (2012) Asphalt, Water, and the Prebiotic Synthesis of Ribose, Ribonucleosides, and RNA. *Accounts of Chemical research* 45:2025–2034.
41. Schopf JW, Kudryavtsev, AB, Agresti, DG, Wdowiak TJ, Czaja AD (2002) Laser-Raman imagery of Earth's earliest fossils. *Nature* 416:73-76.
42. Manning CE, Mojzsis, SJ, Harrison, TM (2006) Geology, Age and Origin of Supracrustal Rocks at Akilia, West Greenland. *American Journal of Science* 306:303-366.
43. Haggerty, SE, Raber E, Naeser CW (1983) Fission track dating of kimberlitic zircons. *Earth and Planetary Science Letters*, 63: 41-50.
44. Ickert RB, Williams IS (2011) U–Pb zircon geochronology of Silurian–Devonian granites in southeastern Australia: implications for the timing of the Benambran Orogeny and the I–S dichotomy. *Australian Journal of Earth Sciences* 58: 501-516
45. Roddick JC, Compston W (1977) Strontium isotopic equilibriation: a solution to a paradox. *Earth and Planetary Science Letters* 34:238-246.
46. Williams IS (1992) Some observations on the use of zircon U-Pb geochronology in the study of granitic rocks. *Second Hutton Symposium: The Origin of Granites and Related Rock*s 83:447-458
47. Chen YD, Williams IS (1990) Zircon inheritance in mafic inclusions from Bega batholith granites, southeastern Australia: An ion microprobe study. *Journal of Geophysical Research* 95(B11):17787
48. Chappell BW, White AJR, Williams IS (1990) Excursion Guide B-1. Cooma Granidiorite and Berridale Batholith. *Seventh International Conference on Geochronology, Cosmochronology, and Isotope Geology*: 1-53.
49. Chappell BW, White AJR (1974) Two contrasting granite types. *Pacific Geology* 8, 173–174.

50. Trail D, Tailby ND, Sochko M, Ackerson MR (2015) Possible Biosphere-Lithosphere Interactions Preserved in Igneous Zircon and Implications for Hadean Earth. *Astrobiology*, 15: 575-86.
51. Trail D, Tailby ND, Wang Y, Harrison, TM, Boehnke P (2017) Aluminum in zircon as evidence for peraluminous and metaluminous melts from the Hadean to present. *Geochemistry, Geophysics, Geosystems* 10.1002/2016GC006794 1-14.
52. Trail D., et al. (2015) Redox evolution of silicic magmas: Insights from XANES measurements of Ce valence in Bishop Tuff zircons. *Chemical Geology*, 402: 77-88.
53. Trail D, *et al.* (2007) Constraints on Hadean zircon protoliths from oxygen isotopes, Ti-thermometry, and rare earth elements. *Geochemistry, Geophysics, Geosystems* 8(6).
54. Georg RB, Reynolds BC, Frank M, Halliday AN (2006) New sample preparation techniques for the determination of Si isotopic compositions using MC-ICPMS. *Chemical Geology*, 235: 95-104.
55. Savage PS, Moynier F. (2013) Silicon isotopic variation in enstatite meteorites: Clues to their origin and Earth-forming material. *Earth and Planetary Science Letters*, 361: 487-496.
56. Young ED, Galy A, Nagahara H. (2002) Kinetic and equilibrium mass-dependent isotope fractionation laws in nature and their geochemical and cosmochemical significance. *Geochimica et Cosmochimica Acta*, 66: 1095–1104.
57. Bindeman IN, Bekker A, Zakharov O (2016) Oxygen isotope perspective on crustal evolution on early Earth: A record of Precambrian shales with emphasis on Paleoproterozoic glaciations and Great Oxygenation Event. *Earth and Planetary Science Letters*, 437, 101-113
58. Valley JW, Kitchen N, Kohn MJ, Niendorf CR, Spicuzza MJ (1995) UWG-2, a garnet standard for oxygen isotope ratios: Strategies for high precision and accuracy with laser heating. *Geochimica et Cosmochimica Acta*, 59: 5223-5231
59. Liu M-C, McKeegan KD, Harrison TM, Jarzebinski G, Vltava L (2018) The Hyperion-II radio-frequency oxygen ion source on the UCLA ims1290 ion microprobe: Beam characterization and applications in geochemistry and cosmochemistry. *International Journal of Mass Spectrometry*, 424: 1-9

Figure legends

Figure 1. Schematic cartoon of Si and O isotope co-variation during fluid alteration and precipitation processes. Chemical weathering, hydration, seawater silica precipitation, may have different trajectories in Si-O isotope space (BSE = Bulk Silicate Earth). Note that 'non-equilibrium silicification' has no specific vector or slope as this process can be highly variable due to the different behavior of these elements under different rock/water ratios and at different temperatures (19). Banded Iron Formations may be enriched in ^{18}O and depleted in ^{30}Si (not shown).

Figure 2. Our MC-ICP-MS results showing that mantle-derived zircon megacrysts Mud Tank carbonatite (Australia), Kimberley pool (South Africa), and Orapa Kimberlite (Botswana) yield an average $\delta^{30}Si$ value of -0.38±0.02 ‰ (1 s.d.). The top of the figure shows the Si isotopic

difference between zircon, quartz, and WR for the LFB I-type Jindabyne tonalite analyzed here; Δ^{30}Si(WR-zircon) is 0.37 ‰.

Figure 3. Histograms showing δ^{30}Si differences of zircons from 10 LFB granitoids and the Duluth Gabbro (SI Appendix, Table S3). The bin sizes are 0.2 ‰, commensurate with the 1 s.e. of our ion microprobe measurements. Some S-types contain measured δ^{30}Si values down to -1.5 ‰, while W060, for example, is largely indistinguishable from the δ^{30}Si of our I-type samples. The A-type and zircons show broadly restricted ranges in δ^{30}Si, when compared to S- and I-type zircons. Whole Rock δ^{30}Si for S-, I-, and A-type LFB granitoids (21) can be found in Fig S1. The mantle zircon field is -0.38±0.02 ‰, after Figure 2. Histograms for zircon δ^{18}O values from individual hand samples can be found in SI Appendix, Fig. S3.

Figure 4. Zircon LFB δ^{18}O vs. δ^{30}Si, with annotated path trajectories after Figure 1. The 'mantle' zircon fields are +5.3±0.3 ‰ and -0.38±0.02 ‰ for δ^{18}O (26) and δ^{30}Si (Fig. 2), respectively. Average δ^{18}O values for S-type zircons are +8.8 ‰, consistent with a whole rock value of δ^{18}O >10 ‰ (28). The zircon δ^{18}O values from I-type rocks yield average values +7.5 ‰, consistent with WR values of <10 ‰ (SI Appendix, Table S3). Path 2 may also indicate a balance between assimilation/derivation between chert-like, "path 3" and pelite-like "path 1" protoliths, both of which have high δ^{18}O.

Figure 5 (a) Plot of δ^{30}Si vs. δ^{18}O for single Hadean (≥4.0 Ga) and Archean zircon, with schematic weathering paths from Figure 1, revealing isotopic heterogeneities in both age suites. Mantle-derived zircon yield values of +5.3±0.3 (26) and −0.38±0.02 ‰ (Fig. 1) for δ^{18}O and δ^{30}Si, respectively. **(b)** Zircon δ^{30}Si plotted against age showing fractionations away from mantle values. Error bars are 1 s.e. (SI Appendix, Table S4) or the standard deviation of multiple ion microprobe analyses on a single grain, whichever is larger. The 'mantle' zircon field is drawn – and reliant upon – high precision MC-ICP-MS data zircon results (SI Appendix, Table S2).

Figure 1

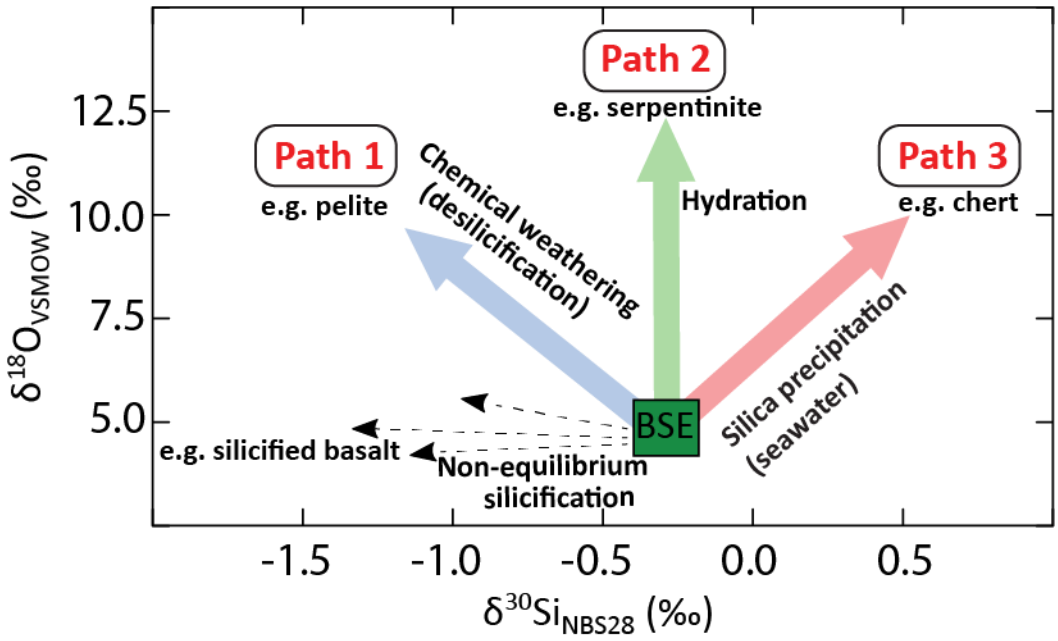
Path 2
e.g. serpentinite
Path 1
e.g. pelite
Path 3
e.g. chert
Chemical weathering
(desilicification)
Hydration
Silica precipitation
(seawater)
BSE
e.g. silicified basalt
Non-equilibrium
silicification
12.5
10.0
7.5
5.0
-1.5
-1.0
-0.5
0.0
0.5
δ18OVSMOW (‰)
δ30SiNBS28 (‰)

Figure 2

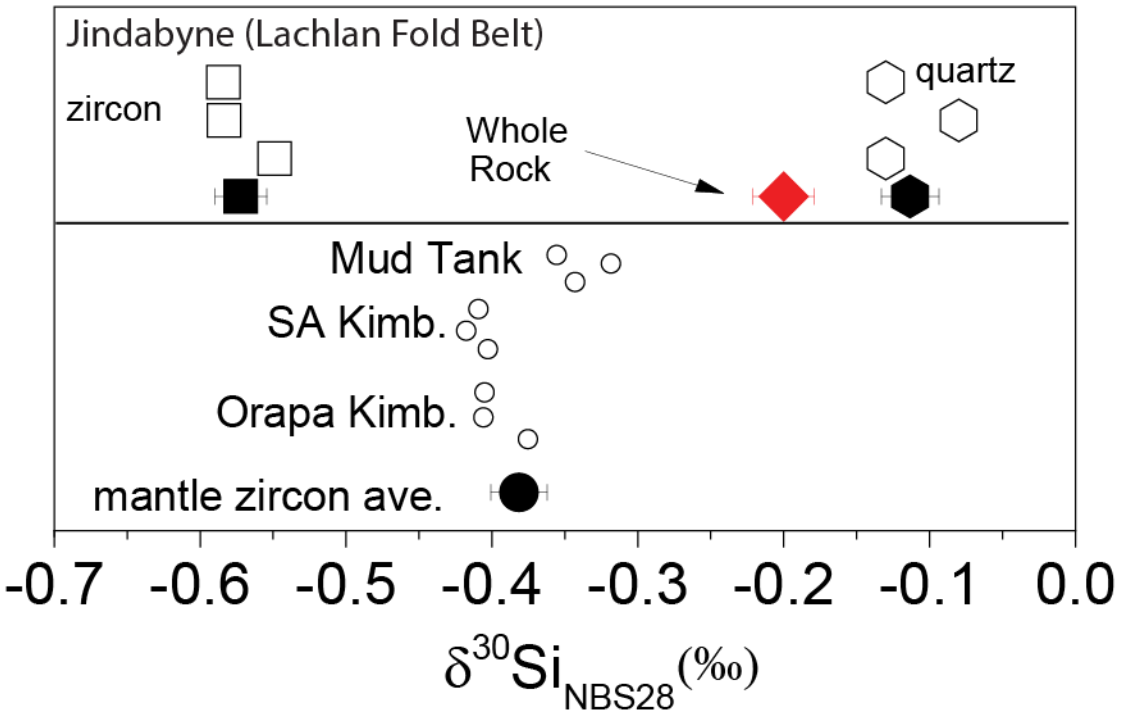
Jindabyne (Lachlan Fold Belt)
zircon
quartz
Whole
Rock
Mud Tank
SA Kimb.
Orapa Kimb.
mantle zircon ave.
-0.7
-0.6
-0.5
-0.4
-0.3
-0.2
-0.1
0.0
δ30SiNBS28 (‰)

Figure 3

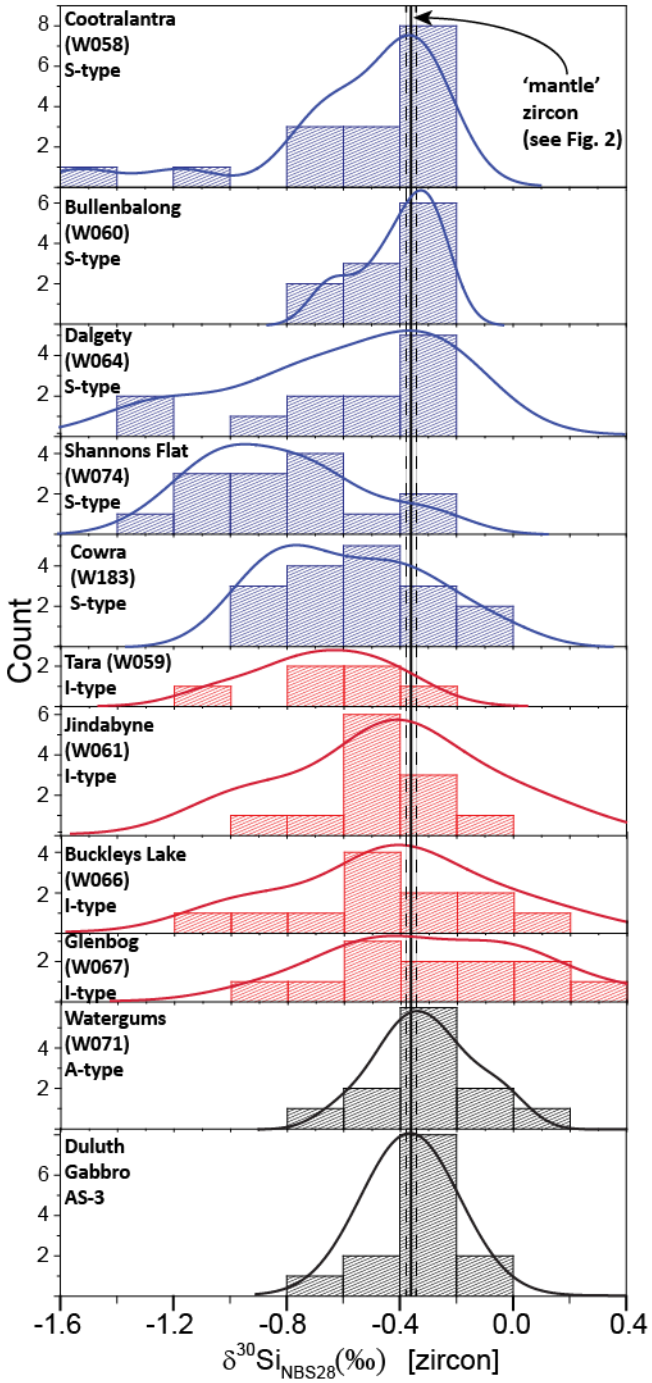
Cootralantra
(W058)
S-type
'mantle'
zircon
(see Fig. 2)
Bullenbalong
(W060)
S-type
Dalgety
(W064)
S-type
Shannons Flat
(W074)
S-type
Cowra
(W183)
S-type
Tara (W059)
I-type
Jindabyne
(W061)
I-type
Buckleys Lake
(W066)
I-type
Glenbog
(W067)
I-type
Watergums
(W071)
A-type
Duluth
Gabbro
AS-3
Count
-1.6
-1.2
-0.8
-0.4
0.0
0.4
δ30SiNBS28(‰) [zircon]

Figure 4

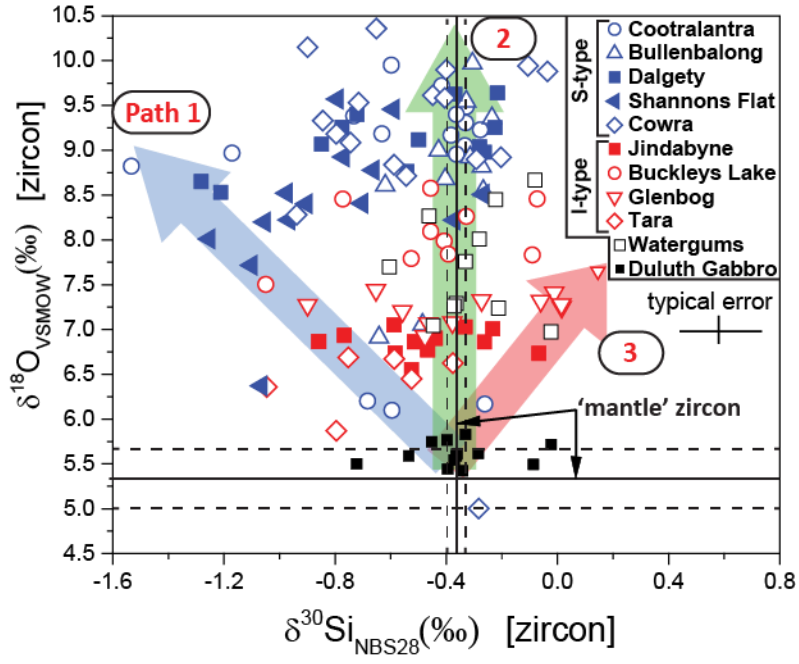
Path 1
2
3
'mantle' zircon
typical error
S-type
I-type
Cootralantra
Bullenbalong
Dalgety
Shannons Flat
Cowra
Jindabyne
Buckleys Lake
Glenbog
Tara
Watergums
Duluth Gabbro
δ18OVSMOW(‰) [zircon]
δ30SiNBS28(‰) [zircon]
10.5
10.0
9.5
9.0
8.5
8.0
7.5
7.0
6.5
6.0
5.5
5.0
4.5
-1.6
-1.2
-0.8
-0.4
0.0
0.4
0.8

Figure 5

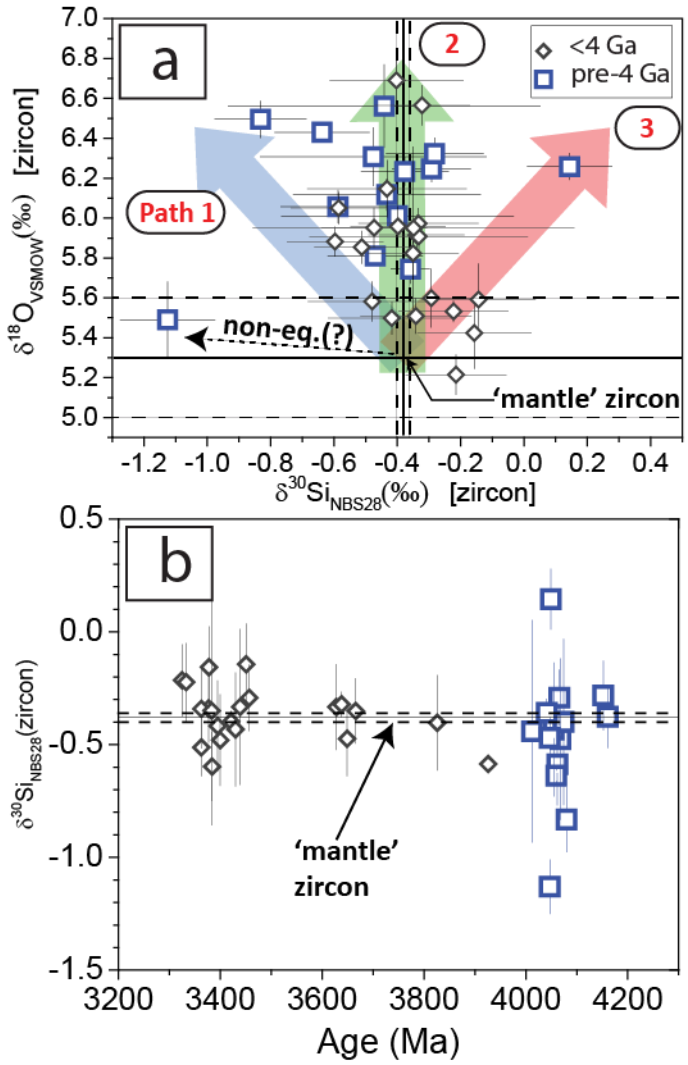
a
b
2
3
<4 Ga
pre-4 Ga
Path 1
non-eq.(?)
'mantle' zircon
$\delta^{18}O_{VSMOW}$(‰) [zircon]
$\delta^{30}Si_{NBS28}$(‰) [zircon]
$\delta^{30}Si_{NBS28}$(zircon)
'mantle' zircon
Age (Ma)